Journal of Catalysis **185,** 120–130 (1999)
Article ID jcat.1999.2497, available online at http://www.idealibrary.com on IDEAL®

# Cobalt Cluster Effects in Zirconium Promoted $Co/SiO_2$ Fischer–Tropsch Catalysts

Andreas Feller, Michael Claeys, and Eric van Steen

*Catalysis Research Unit, Department of Chemical Engineering, University of Cape Town, Private Bag, Rondebosch 7701, South Africa*

Received November 2, 1998; revised March 18, 1999; accepted March 19, 1999

**The effect of zirconium addition to the catalyst formulation of $Co/SiO_2$ Fischer–Tropsch catalysts was investigated. With increasing zirconium content the strong interaction between silica and cobalt is reduced and a somewhat weaker cobalt–zirconium interaction is observed. Therefore the degree of reduction of catalysts, which were reduced at 400°C for 16 h, increases strongly. The cobalt crystallite size increases with increasing zirconium content, leading to smaller cobalt metal surface areas for the freshly reduced catalyst. Cobalt particles can be found in clusters on the silica support. The size of cobalt clusters decreases and thus the number of cobalt particles within a cluster decreases with increasing zirconium content. At steady-state conditions the CO-conversion of the promoted catalyst in the Fischer–Tropsch synthesis increases with increasing zirconium content. The $C_{5+}$-selectivity and the secondary hydrogenation activity pass a maximum with increasing zirconium content. The observed changes in activity and selectivity are explained in terms of an increase in the amount of metallic cobalt available under reaction conditions, leading to an increased activity, and a decrease in the cobalt cluster size, which diminishes the probability for secondary reactions. Furthermore, it was concluded that secondary double bond isomerization can be catalyzed to some extent by zirconia.** 

*Key Words:* **cobalt; zirconium; silica; Co particle size; cluster size; Fischer–Tropsch synthesis; secondary reactions.**

## 1. INTRODUCTION

Metallic cobalt is an excellent catalyst for CO hydrogenation yielding higher hydrocarbons (Fischer–Tropsch synthesis) (1, 2), especially when high chain growth probability and a low branching probability are required (3). The activity of supported cobalt catalysts in the Fischer–Tropsch synthesis should be proportional to the area of the exposed metallic cobalt atoms (4, 5). A requirement for highly active Co-catalyst is therefore a high dispersion of the cobalt metal. This is usually done by deposition of a cobalt salt on high surface area supports, such as silica and alumina and subsequent reduction.

Cobalt ions interact strongly with commonly used support materials such as alumina (6) and silica (7–13) yielding species which can be reduced only at elevated temperatures (exceeding 1000 K). On silica these species are thought to be cobalt silicates and cobalt hydrosilicates (7–12), although they could not be identified unambiguously using EXAFS (13). The role of these species in supported cobalt catalysts is not clear. It has been indicated (11) that a certain amount of these cobalt silicates is necessary to obtain highly dispersed cobalt catalysts. This has been shown for $Ni/SiO_2$, where nickel hydrosilicate species, which are more difficult to reduce, act as "anchors" for reduced nickel crystallites (14).

The promotion of supported cobalt catalyst with noble metals, transition metal oxides, and rare earth oxides have been reviewed recently (15). Only a few studies focused on the promotion of supported cobalt catalysts with zirconium (5, 16–19). It has been claimed that zirconium enhances the activity of $Co/SiO_2$ catalysts (16–18). Other authors reported no specific effect of zirconium on the intrinsic activity of cobalt catalysts (5, 19). Here, we report the effect of zirconium on the physical properties of $Co/SiO_2$ and their performance in the Fischer–Tropsch synthesis at steady-state.

## 2. EXPERIMENTAL

### *Catalyst Preparation*

The catalysts were prepared by means of incipient wetness. A series of catalysts were prepared to investigate the order of addition and the influence of intermediate drying/calcination steps. The general applied procedure was as follows. Zirconium oxide chloride ($ZrOCl_2 \cdot 8H_2O$ p.a., Merck) was dissolved in an appropriate amount of deionized water and added to 15 g silica (Davisil grade 666; $d_{particle} = 150$–$250$ $\mu$m; $S_{BET} = 480$ m$^2$/g, $d_{pore} = 60$ Å, $V_{pore} = 1.5$ cm$^3$/g). The catalyst precursor was aged at room temperature for 0.3 h and subsequently dried in an oven at 383 K for 16 h. Cobalt nitrate ($Co(NO_3)_2 \cdot 6H_2O$ p.a., Carlo Erba) was dissolved in an appropriate amount of deionized water and added to the catalyst precursor. The catalyst precursor was aged at room temperature for 20 min and subsequently dried in an oven at 383 K for 16 h.



0021-9517/99 $30.00

The composition of the catalysts was checked using AAS and ICP. For that purpose the catalysts were calcined in air at 673 K for 16 h and subsequently dissolved in HF. The cobalt loading for all samples was within the error of measurement 0.085 g Co/g $SiO_2$.

For some characterizations the catalyst precursor was calcined by heating the sample at 10 K/min in a nitrogen or air flow (60 ml (NTP)/min) up to 673 K and held at this temperature for 1 h. The calcination step was then immediately followed by the characterization. The calcination step was included for nitrate decomposition (the calcination atmosphere does not influence the obtained TPR spectra (12)).

Generally, the catalyst samples were reduced directly without an intermediate calcination step. The reduction was carried out in a fixed bed reactor. The catalyst precursor (2.5 g) was loaded into the isothermal zone of the reduction reactor. The samples were heated at 10 K/min in a hydrogen flow (60 ml (NTP)/min) up to 673 K and held at this temperature for 16 h. Subsequently, the reactor was cooled down to room temperature and the catalyst was slowly exposed to air. This caused some surface oxidation and necessitated a rereduction of the catalyst before characterization/reaction.

### *Temperature Programmed Reduction (TPR)*

The catalyst precursor and the reduced catalyst samples were characterized using TPR. These experiments were performed in home-built equipment which had been described previously (12). Briefly, 0.15 g of catalyst was loaded into the quartz cell. TPR was performed by heating the sample with 10 K/min from 373 K up to 1273 K using 60 ml (NTP)/min of 5 vol% $H_2$ in a $N_2$ mixture. The temperature was held at the final temperature for 0.5 h. The concentration of hydrogen was monitored using a TCD after removal of the product water using a 3-Å molecular sieve. The TPR was calibrated using the reduction of NiO.

### *Metal Surface Area, Dispersion, and Cobalt Crystallite Size*

Metal surface and the cobalt dispersion of the catalysts were determined using $H_2$-chemisorption using a Micrometrics ASAP 2000 Chemisorption apparatus. The procedure involved a rereduction of ca. 1 g of the reduced sample at 473 K for 4 h in hydrogen (60 ml (NTP)/min). Following reduction, the sample holder was evacuated at 473 K for 2 h. The catalyst was cooled down under vacuum to adsorption temperature (373 K) (20) and evacuated for another 3 h. The pressure was then less than 0.1 Pa. The adsorption isotherm was measured between 6 and 40 kPa. For the calculation of the average particle diameter it was assumed that reduced cobalt and nonreduced cobalt form different phases (21). Using a density of 8.9 g/$cm^3$ and assuming spherical metallic cobalt particles the average particle size was calculated.

Cobalt crystallite size was also determined by line width broadening in XRD-pattern using a Philips PW1390 diffractometer. The analysis was performed using Co $K\alpha$ radiation. The spectrum between $2\theta = 20^\circ$ and $2\theta = 60^\circ$ was recorded using a step size of $0.05^\circ$.

Transmission electron microscopy (TEM) characterization of the samples was carried out using a JEOL JEM-200CX instrument operating at 200 kV. The samples were crushed in an agate mortar, using acetone. Thin slices were prepared which were supported on copper grids. At least three TEM images were taken to evaluate the cobalt crystallite size and the formation of clusters of cobalt particles. Thus, only a rough indication on the size of the cobalt clusters can be given, due to the limited number of TEM images.

### *Reaction Studies*

The Fischer–Tropsch synthesis was performed in a downflow fixed bed reactor at 463 K and 5 bar. A glass reactor was mounted inside a stainless steel mantle. Catalyst (1 g) was loaded into the isothermal zone of the reactor and the catalyst was rereduced in $H_2$ (60 ml(NTP)/min) at 473 K for 4 h, after which the catalyst was cooled down to reaction temperature (463 K) and pressurised under argon (5 bar). The temperature was measured and controlled in the middle of the catalyst bed. The catalyst was located in an annular ring surrounding the thermo-well ($d_{in} = 3$ mm; $d_{out} = 10$ mm). The length of the catalyst bed was approximately 8–10 mm. The flow of each of the reagents, hydrogen and carbon monoxide ($H_2 : CO = 2 : 1$), was controlled using mass flow controllers. Argon was added after the reactor to the product stream to maintain the reaction pressure. After the pressure release valve a flow of cyclohexane in nitrogen was added to the product stream as an internal standard. Samples of the product stream were taken using the ampoule sampling technique (22).

The organic product compounds were separated using a 50-m OV-1 column ($d_i = 0.2$ mm, $d_f = 0.2$ $\mu$m) employing a temperature program from 203 to 553 K. The products were analyzed using a FID. The inorganic gases were separated isothermally at 333 K using a 3-m × 6.4-mm Carbosieve column and analyzed using a TCD.

## 3. RESULTS

### *Temperature Programmed Characterization of Calcined Samples*

Figure 1 shows the TPR spectra obtained for the calcined, zirconium promoted Co/$SiO_2$ catalyst precursors. The hydrogen consumption associated with the reduction is between 1.04 and 1.4 mol $H_{2,consumed}$/mol Co and tends to decrease with increasing zirconium loading. The sample without zirconium shows the typical reduction behavior of Co/$SiO_2$ (9–12). The sharp maximums at low temperatures

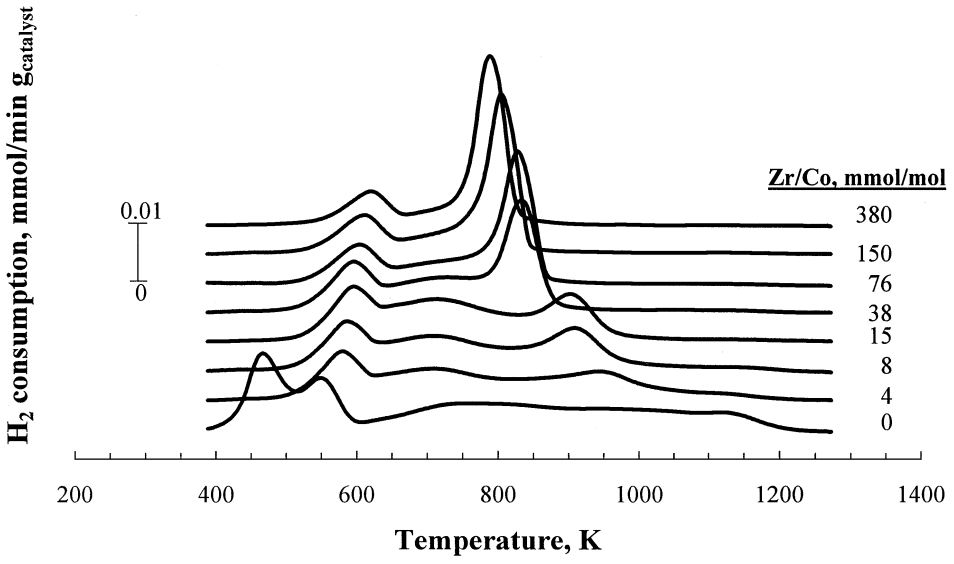


**FIG. 1.** Influence of zirconium loading on the reduction behavior of zirconium promoted $Co/SiO_2$ ($m_{catalyst} \approx 0.15$ g; Co-loading, 0.085 g Co/g $SiO_2$; calcination, 673 K for 1 h in $N_2$ (60 ml (NTP)/min; reducing gas, 5% $H_2/N_2$ (60 ml (NTP)/min); heating rate, 10 K/min).

can be attributed to the two-step reduction process of $Co_3O_4$ ($Co(III)_2Co(II)O_4 \rightarrow Co(II)O \rightarrow Co$) (6). The reduction of $Co_3O_4$ is followed by a broad region of hydrogen consumption, which can tentatively be ascribed to the reduction of cobalt hydrosilicates and cobalt silicates. Upon addition of zirconium to the catalyst formulation the first, low temperature reduction peak disappears. This might indicate that zirconium promoted $Co/SiO_2$ contains much less $Co_3O_4$. The second maximum shifts toward higher temperatures, indicating a higher resistance against reduction. This might be ascribed to a weak interaction between divalent cobalt and zirconium. The most pronounced difference is observed in the high temperature region, where the broad region of hydrogen consumption is replaced by a sharp maximum in the rate of hydrogen consumption. This can be ascribed to an interaction between cobalt and zirconium, which replaces the cobalt–silica interaction. It is further observed that the amount of hydrogen consumed for the high temperature reduction increases with increasing zirconium content (from ca. 58% of the total hydrogen consumption for $Zr/Co = 0$ mmol/mol up to 80% for $Zr/Co = 380$ mmol/mol). This indicates a favored interaction of divalent cobalt with zirconium species during the preparation of the catalyst sample.

The order of addition of zirconium oxide chloride and cobalt nitrate and the influence of intermediate drying/calcination steps were also investigated. Four different samples were prepared, in which the order of addition of Co and Zr was changed and the intermediate calcination step was added (see Fig. 2).

The intermediate calcination markedly alters the TPR spectra of the differently prepared samples. The sample, which was first impregnated with $ZrOCl_2$ and then dried and calcined and subsequently impregnated with cobalt nitrate (sample A), shows a reduction behavior similar to that of $Co/SiO_2$. During calcination $ZrOCl_2$ is transformed into $ZrO_2$ (23). This indicates that during impregnation divalent Co ions are more likely to interact with silica than with zirconia. If the order of impregnation is changed (but keeping the intermediate calcination step—sample B), a small interaction with between Co and zirconium can be observed. This indicates that $ZrOCl_2$ can replace the interaction between Co and silica. A much more pronounced interaction between Co and zirconium is observed if the intermediate calcination step is omitted (samples C and D). This indicates that the cobalt–zirconium interaction is formed due to an interaction between the zirconium salt and cobalt ions.

### *Temperature Programmed Reduction of Reduced Samples*

Figure 3 shows the TPR-spectra obtained from the catalyst samples reduced at 673 K for 16 h in flowing hydrogen. The spectra are characterized by a low temperature region of hydrogen consumption and a high temperature region of hydrogen consumption. The low temperature region of hydrogen consumption can be ascribed to the reduction of surface cobalt oxides, which were formed during the exposure of the catalysts to air. The high temperature region of hydrogen consumption can be ascribed to the reduction of species, which were not reduced during the reduction at 673 K.

Table 1 shows the hydrogen consumption associated with the two regions of reduction. With increasing zirconium content the amount of hydrogen consumed for the low temperature reduction decreases. Since the low temperature reduction process is the reduction of surface oxide, this

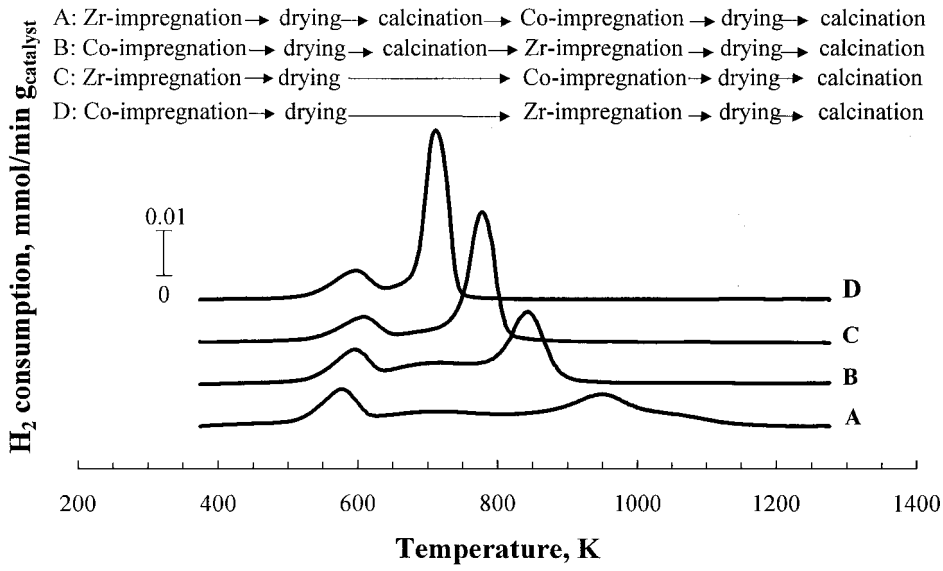


**FIG. 2.** Influence of the preparation procedure of the samples on the reduction behavior of zirconium promoted Co/$SiO_2$ catalysts ($m_{catalyst} \approx 0.15$ g; Co-loading, 0.085 g Co/g $SiO_2$; Zr-loading, 380 mmol Zr/mol Co; drying, at 383 K for 16 h; calcination, 673 K for 16 h in air; reducing gas, 5% $H_2/N_2$ (60 ml (NTP)/min); heating rate, 10 K/min).

indicates that with increasing zirconium content the oxidizable surface decreases. The amount of hydrogen consumed during the high temperature reduction also decreases with increasing zirconium content with the exception of the sample with Zr/Co = 15 mmol/mol. This indicates that the degree of reduction of the samples increases with increasing zirconium loading. The deviation observed with the sample Zr/Co = 15 mmol/mol could have been expected on basis of the TPR experiments of the calcined samples. With increasing zirconium loading the interaction between zirconium and cobalt becomes more pronounced. The reducibility of these species becomes better at high zirconium loading as visualized by the decrease in the temperature at which the high temperature hydrogen consumption was maximal. Furthermore, if zirconium is present in the sample, cobalt will interact preferentially with zirconium. This leads to a high degree of interaction between cobalt and zirconium in the sample with Zr/Co = 15 mmol/mol. The reduction of these cobalt–zirconium species requires a high temperature at this low zirconium loading. In this sample cobalt bound in these species can thus hardly be reduced at 673 K.

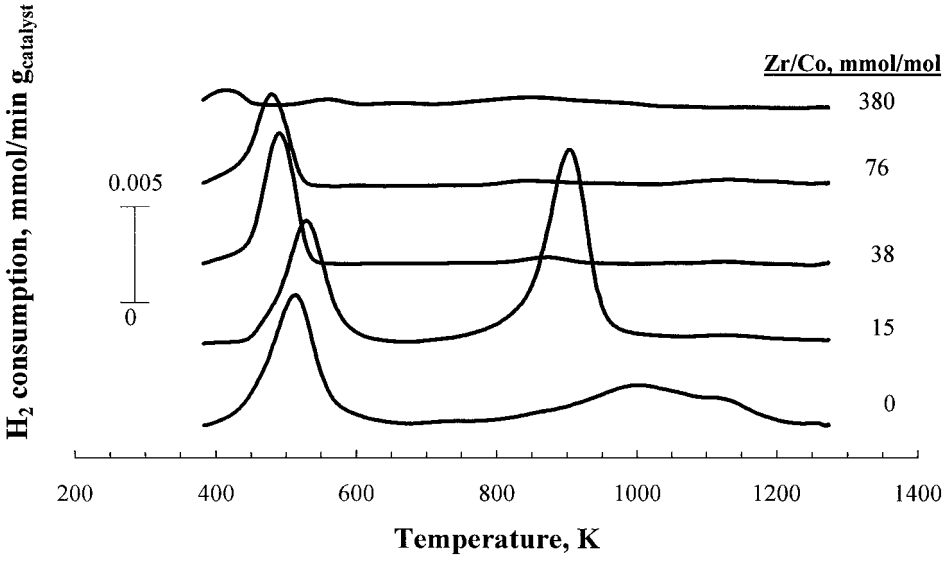


**FIG. 3.** Influence of zirconium on the reduction behavior of reduced, zirconium promoted Co/$SiO_2$ catalysts ($m_{catalyst} \approx 0.15$ g; Co-loading, 0.085 g Co/g $SiO_2$; reduction, 673 K for 16 h in $H_2$ (60 ml (NTP)/min); reducing gas during TPR, 5% $H_2/N_2$ (60 ml (NTP)/min); heating rate, 10 K/min).

**TABLE 1**

**Hydrogen Consumption during TPR of the Reduced, Zirconium Promoted $Co/SiO_2$ Samples ($T_{reduction} = 673$ K; $t_{reduction} = 16$ h)**

| Zr/Co (mmol/mol) | $H_2$ consumption below 673 K (mol $H_2$/mol Co) | $H_2$ consumption above 673 K (mol $H_2$/mol Co) | Total $H_2$ consumption (mol $H_2$/mol Co) |
|---|---|---|---|
| 0 | 0.30 | 0.29 | 0.59 |
| 15 | 0.28 | 0.56 | 0.84 |
| 38 | 0.22 | 0.06 | 0.28 |
| 76 | 0.16 | 0.06 | 0.22 |
| 380 | 0.03 | 0.05 | 0.08 |

*Metal Surface Area, Crystal Size, and Dispersion*

The results obtained using hydrogen chemisorption, X-ray diffraction, and transmission electron microscopy are summarized in Table 2. With increasing zirconium content in the samples the crystallite size of reduced cobalt metal increases significantly. This could already be concluded on basis of the temperature programmed reduction experiments with the reduced samples, in which a decrease of the low temperature hydrogen consumption with increasing zirconium content was observed. The low temperature hydrogen consumption was attributed to a surface oxidation of reduced, zero valent cobalt. The decrease in the hydrogen consumption thus relates to a decrease in the metal particle size and thus to an increase in metal particle size as observed using $H_2$-chemisorption, XRD, and TEM.

The TEM images (see Fig. 4) show that cobalt particles are present as clusters. With increasing zirconium content the cobalt metal particle size increases, but the cluster size decreases. TEM images of $Co/SiO_2$ ($Zr/Co = 0$) before reduction, showed the presence of droplets of cobalt nitrate. The size of these droplets was similar to the size of the cobalt cluster in the reduced sample. It is indicated that the cobalt–zirconium interaction favors the distribution of Co over the whole silica particle.

*Reaction Study*

Figure 5 shows a typical time-on-stream curve for the catalysts investigated. After 24 h on stream a steady state for the formation of products was obtained. The catalysts were evaluated at after 24 h on stream. Table 3 summarizes the activity and selectivities in the Fischer–Tropsch synthesis at 463 K and 5 bar ($H_2/CO = 2$) obtained with the rereduced samples. The steady-state conversion increases with increasing zirconium content, except for the catalyst with $Zr/Co = 15$ mmol/mol. The turnover frequency follows the same trend.

Methane selectivity and the selectivity of the $C_{5+}$-fraction follow opposite trends and show a minimum and a maximum respectively at a Zr to Co ratio of 15 mmol/mol. The observed chain growth probabilities confirm that the difference between CO conversion and the yield of volatile organic products can be ascribed to the formation of wax.

With increasing zirconium loading the olefin content in the $C_2$-fraction passes a minimum. An extremely high ethene to ethane ratio of 6 was observed for the catalysts with a high zirconium loading. This indicates that secondary hydrogenation is strongly inhibited at high zirconium loading. The olefin content in the $C_3$-fraction follows a similar trend although much less pronounced. This can be ascribed to the difference in the reactivity between propene and ethene (24). An olefin content in the fraction of linear hydrocarbons of 85–86% seems to be the primary selectivity for the Fischer–Tropsch synthesis at these conditions.

The influence of zirconium loading on the fraction of $C_5$ hydrocarbons was investigated in detail. The ratio of branched $C_5$ hydrocarbons to linear $C_5$ hydrocarbons varies

**TABLE 2**

**Physio-chemical Characteristics of Reduced Zirconium Promoted $Co/SiO_2$ Catalysts ($Co/SiO_2 = 0.085$ g/g; $T_{reduction} = 673$ K, $t_{reduction} = 16$ h; reducing gas: $H_2$ 60 ml(NTP)/min)**

| Zr/Co (mmol/mol) | %Reduction[a] | $H_2$ Chemisorption: $H_{2,\,adsorbed}$ (mmol/mol Co)[b] | $H_2$ Chemisorption: Metal surface area ($m^2$/g catalyst) | $H_2$ Chemisorption: Dispersion (%) | Crystal size (nm): $H_2$ chemisorption | Crystal size (nm): XRD | Crystal size (nm): TEM | Cluster size (nm), TEM |
|---|---|---|---|---|---|---|---|---|
| 0 | 71 | 39 | 3.5 | 7.8 | 12 | 12 | ca. 10 | 60–100 |
| 15 | 44 | 19 | 1.1 | 3.9 | 25 | 15 | 5–20 | 50–80 |
| 38 | 94 | 21 | 2.4 | 4.1 | 23 | 19 | 5–20 | 30–50 |
| 76 | 94 | 14 | 1.6 | 2.8 | 35 | 26 | — | — |
| 380 | 95 | 10 | 1.1 | 1.9 | 51 | 29 | 30–50 | — |

[a] Degree of reduction determined on the basis of the amount of hydrogen consumed at high temperatures in the TPR experiments using reduced catalyst samples.

[b] Amount of hydrogen adsorbed per mol of reduced cobalt metal present in sample.

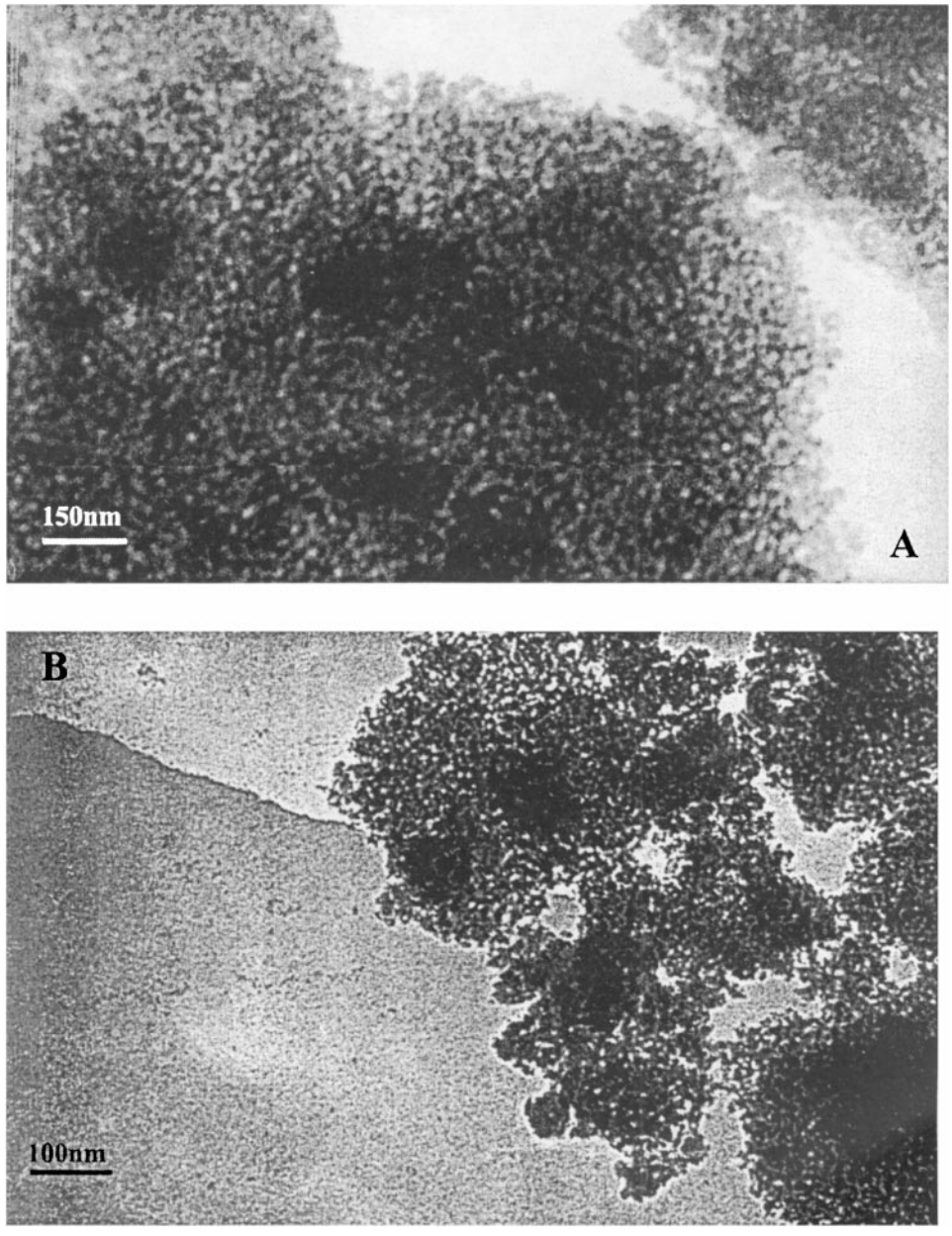


**FIG. 4.** Transmission electron microscopy (TEM) images of reduced samples ($Co/SiO_2 = 0.085$ g/g) with varying zirconium content. (A) 0 mmol Zr/mol Co; (B) 15 mmol Zr/mol Co; (C) 38 mmol Zr/mol Co; (D) 76 mmol Zr/mol Co; (E) 380 mmol Zr/mol Co.

between 2.2 and 4.6 mol%. A significant trend as a function of zirconium content could not be observed. Figure 6 shows the influence of zirconium loading on the olefin content in the fraction of linear and branched $C_5$ hydrocarbons and on the $\alpha$-olefin content in the fraction of linear and branched $C_5$ olefins. The observed trend for the olefin content in the fraction of linear hydrocarbons is similar to that observed for the $C_2$- and $C_3$-fractions. The olefin content in the fraction of branched hydrocarbons increases with increasing zirconium content. The olefin content in the fraction of branched hydrocarbons is generally lower than that in the fraction of linear hydrocarbons. A lower primary olefin selectivity in the fraction of branched hydrocarbons has been observed before (25) and was rationalized on basis of the number of H atoms in $\beta$-position.

The $\alpha$-olefin content in both fractions decreases with increasing zirconium loading, indicating a larger extent of double bond isomerization with increasing zirconium content. The $\alpha$-olefin content in the fraction of branched $C_5$-olefins is lower than that in the fraction of linear $C_5$-olefins. The lower $\alpha$-olefin content in the fraction of branched $C_5$-olefins than in the fraction of linear $C_5$-olefins must be

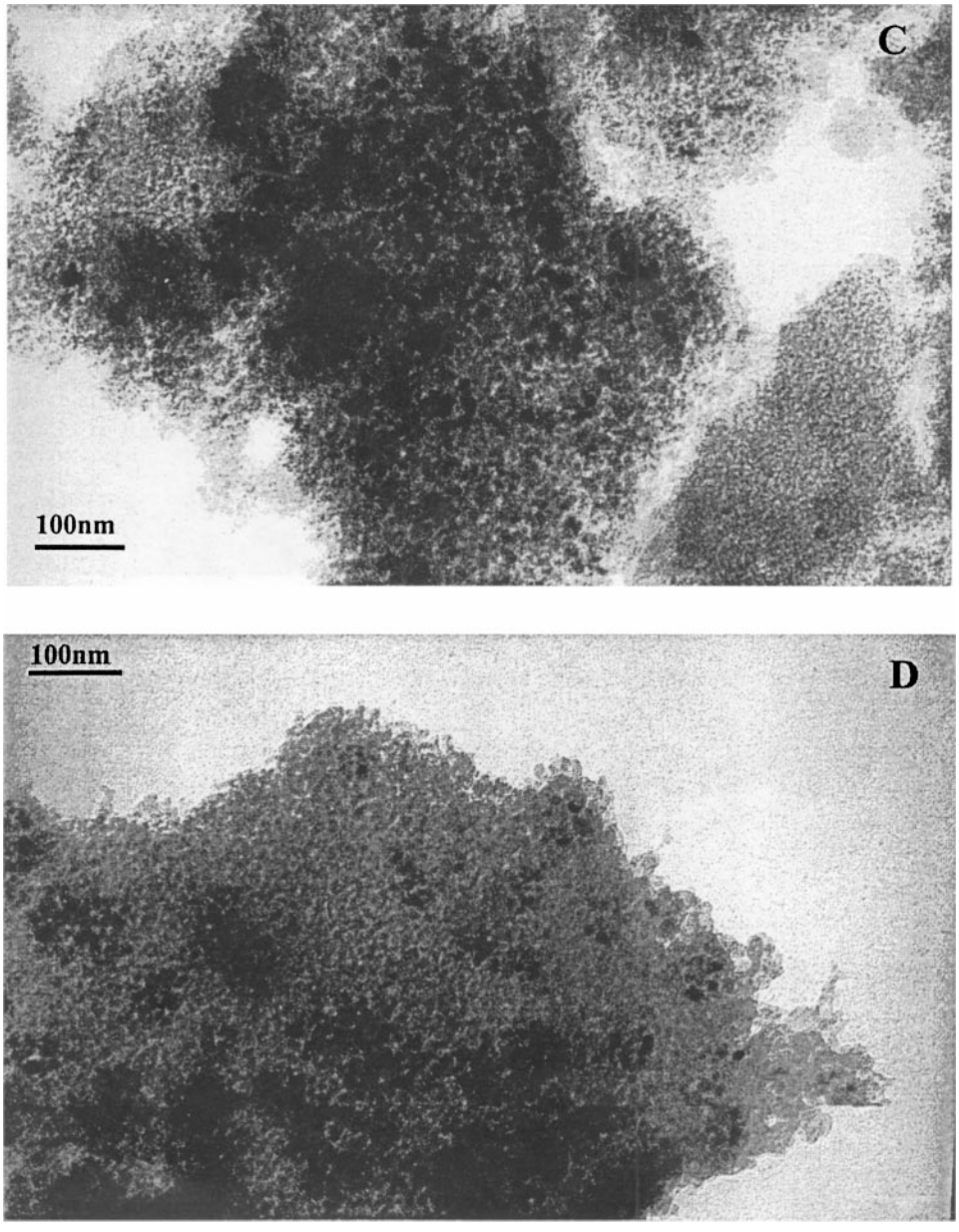


**FIG. 4**—*Continued*

ascribed to a higher activity of 3-methyl-1-butene for double bond isomerization than 1-pentene (25).

## 4. DISCUSSION

The addition of zirconium oxide chloride to $Co/SiO_2$ catalyst formulation modifies the interaction of cobalt with silica and a distinct cobalt–zirconium species is formed. The cobalt–zirconium species might be formed during impregnation or drying, since the TPR spectra of the samples in which the order of addition was changed, were similar. It is possible that during the second impregnation step the salt, which was added to silica first, dissolves. If zirconium oxide chloride is added first, followed by calcination before the impregnation with cobalt nitrate the interaction between zirconia and cobalt is negligible. Above 493 K $ZrOCl_2 \cdot 8H_2O$ is transformed into $ZrO_2$ (23). This shows that the zirconium salt is necessary to form a cobalt-zirconium interaction.

The cobalt–zirconium species can be reduced at lower temperatures than cobalt silicates, leading to a significant higher degree of reduction in the reduced catalysts. All three methods of determining the cobalt crystallite size show that the cobalt metal particle size increases with increasing zirconium content due to the interaction between zirconium and cobalt.

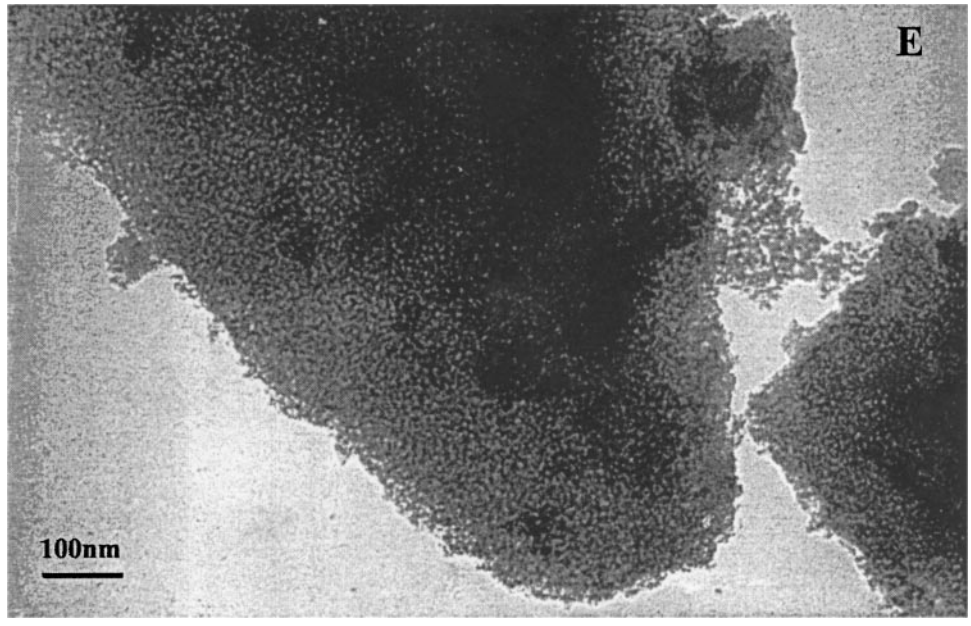


**FIG. 4**—*Continued*

Cobalt particles in Co/$SiO_2$ are present in clusters. TEM showed that the size of the clusters decreases with increasing zirconium content. The cluster size of the unpromoted Co/$SiO_2$ catalyst is determined by the size of the cobalt nitrate droplet during the drying process. TEM images of the unpromoted catalyst showed areas with a high density of cobalt particles and large areas with no cobalt present. TEM images of catalysts with a high zirconium loading showed a more even, but sparse distribution of large cobalt particles.

Significant differences were observed in the activity and selectivity of these catalysts in the Fischer–Tropsch synthesis. The steady-state conversion and turnover frequencies of the catalysts increase with increasing zirconium content. However, the metal surface area of the freshly reduced catalyst decreases with increasing zirconium content. This is surprising since it has been reported that the intrinsic activity of Co atoms is independent of the dispersion (5). It must, however, be kept in mind, that the turnover frequencies were calculated based on the metal surface area of the freshly reduced catalysts. During the CO hydrogenation small cobalt particles can reoxidize (26) and form cobalt silicates (27). The reoxidation of small particles can thus lead to a loss of a number of the active sites. The catalysts investigated in this study have different cobalt particle size distributions. Since it can be expected that the small cobalt particles will not be active any more at steady-state conditions, the relative deactivation of the different catalysts will differ. The turnover

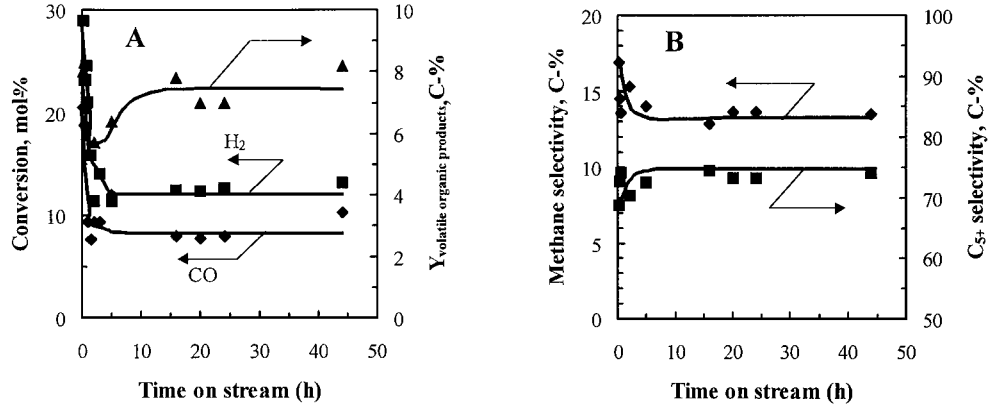


**FIG. 5.** Typical time-on-stream behavior of supported Co/$SiO_2$ catalysts in the Fischer–Tropsch synthesis (catalyst composition, 0.085 g Co/g $SiO_2$; Zr/Co, 15 mmol/mol; reaction conditions: $H_2/CO = 2$; $T_{reaction} = 463$ K; $p_{reaction} = 5$ bar; WHSV = 300 $h^{-1}$). (A) $H_2$ and CO conversion and the yield of volatile organic product compounds as a function of time on stream. (B) Selectivity for methane and $C_{5+}$ as a function of time on stream.

**TABLE 3**

**Influence of Zirconium Content of Catalysts ($Co/SiO_2 = 0.085$ g/g; $T_{reduction} = 673$ K; $t_{reduction} = 16$ h) in the Fischer–Tropsch Synthesis at Steady State ($H_2/CO = 2$; $T_{reaction} = 463$ K; $p_{reaction} = 5$ bar; $t_{reaction} = 24$ h)**

| Zr/Co, mmol/mol | 0 | 15 | 38 | 76 | 380 |
|---|---|---|---|---|---|
| $X_{CO}$ (C-%) | 5.7 | 9.4 | 7.4 | 8.7 | 15.9 |
| TOF[a] ($s^{-1}$) | $0.6 \times 10^{-2}$ | $3.7 \times 10^{-2}$ | $1.1 \times 10^{-2}$ | $2.0 \times 10^{-2}$ | $5.5 \times 10^{-2}$ |
| $Y_{VOP}$ (C-%)[b] | 5.1 | 7.0 | 6.9 | 7.7 | 15.1 |
| $S_{CO_2}$ (C-%) | bd[c] | bd[c] | bd[c] | bd[c] | bd[c] |
| $S_{CH_4}$ (C-%)[d] | 19.2 | 13.7 | 16.4 | 18.4 | 16.8 |
| $S_{C_2}$ (C-%)[d,e] | 2.9 (58) | 2.1 (43) | 3.7 (58) | 7.9 (83) | 11.5 (86) |
| $S_{C_3}$ (C-%)[d,e] | 7.8 (83) | 3.3 (79) | 4.3 (79) | 6.6 (86) | 6.6 (84) |
| $S_{C_4}$ (C-%)[d] | 8.4 | 6.1 | 9.3 | 9.1 | 7.1 |
| $S_{C_{5+}}$ (C-%)[d] | 60.5 | 73.2 | 61.9 | 57.8 | 58.1 |
| $\alpha^f$ | 0.746 | 0.874 | 0.765 | 0.741 | 0.748 |
| $\alpha^g$ | 0.830 | 0.875 | 0.786 | 0.837 | 0.790 |

[a] Turnover frequency based on the metal dispersion of the freshly reduced catalyst.
[b] Yield of volatile organic products ($C_1$–$C_{20}$).
[c] Below detection limit of 0.5 C-%.
[d] Fraction within the fraction of volatile hydrocarbons (HC).
[e] In brackets olefin content in the fraction of linear hydrocarbons.
[f] Chain growth probability in the range $C_3$–$C_7$.
[g] Chain growth probability in the range $C_{10}$–$C_{14}$.

frequency can therefore only be an indication of the overall activity based on the number of metallic cobalt atoms, which were present in the freshly reduced catalyst. If the intrinsic activity of cobalt is independent of the dispersion, the deactivation should decrease with increasing zirconium content; i.e., at steady state the number of surface cobalt atoms increases with increasing zirconium content.

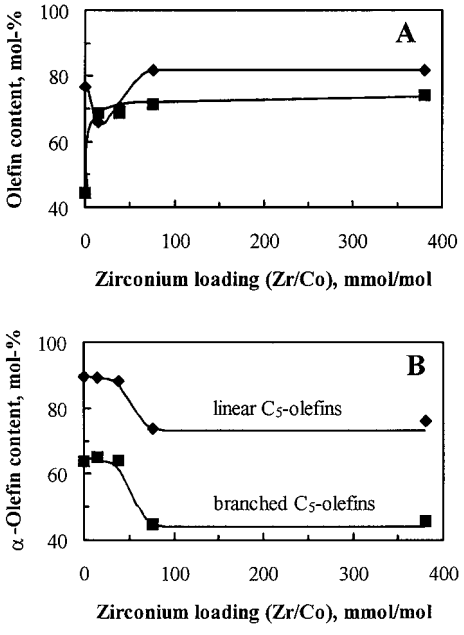


**FIG. 6.** Influence of zirconium loading on the distribution of the $C_5$ hydrocarbons obtained in the Fischer–Tropsch synthesis ($H_2/CO = 2$; $T_{reaction} = 463$ K; $p_{reaction} = 5$ bar; WHSV $= 300$ $h^{-1}$). (A) Olefin content in the fraction of linear and branched $C_5$ hydrocarbons. (B) $\alpha$-Olefin content in the fraction of linear and branched $C_5$-olefins.

With increasing zirconium content the selectivity for $C_{5+}$-fraction passes a maximum and a minimum in the methane selectivity is observed. Cobalt catalysts show a strong tendency for readsorption and incorporation of reactive compounds, such as olefins and alcohols, into growing chains (24, 28, 29). If smaller reactive product compounds, such as ethene and propene, are readsorbed and act as a chain starter, the selectivity of the $C_{5+}$-fraction will increase (29). An increase in the $C_{5+}$ selectivity can thus be interpreted as an increase in the extent of reincorporation of the small reactive organic product compounds into the chain growth mechanism of the Fischer–Tropsch synthesis. Since a maximum in the $C_{5+}$-selectivity is observed, this indicates a dual effect of the catalyst composition on the selectivity of the reaction.

The steady-state activity increases with increasing zirconium content. It is thus expected that the extent of readsorption of small reactive organic product compounds also increases with increasing zirconium content.

The size of the cluster of cobalt particles, however, decreases with increasing zirconium content. The formation of clusters of cobalt particles means that the distribution of cobalt in the catalyst is inhomogeneous. An inhomogeneous distribution of cobalt severely affects the selectivity of the Fischer–Tropsch synthesis.

Suppose, that the conversion of carbon monoxide in the Fischer–Tropsch synthesis and the readsorption of reactive organic product compounds can be very roughly approximated as a consecutive reaction scheme $A \rightarrow B \rightarrow C$

(Type III selectivity according to Wheeler (30)). For argument's sake, it is assumed that both reactions are first order. The selectivity of the final product C is then a function of the ratio of the rate constants and the conversion of the reactant A. If cobalt is homogeneously distributed over the silica particle, the rate constants for both reactions in each pore containing cobalt will be the same. If cobalt is distributed in only half of the pores and the other half of the pores contain no cobalt, the activity per pore containing cobalt will double. The ratio of the rate constants is not affected by the inhomogeneous distribution of cobalt particles. Since the rate constant per pore increases for the conversion of the reactant A, the conversion of A in a pore will increase and thus the selectivity for the final product C in the pore will increase. Integrated over all pores containing the cobalt, this result should not affect the overall conversion of the reactant A (if the reaction is not limited by pore diffusion). The selectivity for the final product C will be enhanced by an inhomogeneous distribution. The extent to which the selectivity for the final product C can be enhanced is larger if the ratio of the rate constant for the formation of C relative to that of the consumption of A is high. The effect is most noticeable if the reaction is carried out without noticeable pore diffusion limitations for the reactant A.

The selectivity for olefins follows the opposite trend of the $C_{5+}$-selectivity and passes a minimum with increasing zirconium content. With increasing zirconium loading, the number of metal sites at steady state increases and thus the probability for secondary hydrogenation would increase. The extent of secondary reactions and thus secondary hydrogenation decreases with decreasing size of the cobalt clusters.

It has been argued that the extent of secondary reactions catalyzed by cobalt passes a maximum with increasing zirconium content (vide supra). This is not observed for the double bond isomerization, which occurs to a large extent on catalysts with a high zirconium content. Double bond isomerization is a very facile reaction and cannot be catalyzed only by metals, but also by metal oxides. The increase in the double bond isomerization can be attributed to the catalytic activity of zirconia.

## 5. CONCLUSIONS

The addition of zirconium oxide chloride to the catalyst formulation of Co/$SiO_2$ was investigated. It leads to a higher reducibility of cobalt, due to the formation of a cobalt–zirconium species, which can be reduced at lower temperatures than cobalt silicate. Furthermore, the metal particle size of cobalt is increased, but the size of cobalt clusters is reduced.

The Co–Zr/$SiO_2$ catalysts were tested for their activity in the Fischer–Tropsch synthesis. The steady-state activity increased with increasing zirconium loading, which was attributed to the resistance against reoxidation of the larger cobalt particles and thus to the larger amount of surface cobalt metal present at steady-state in the zirconium promoted catalysts. Based on the assumption that the intrinsic activity of cobalt in these catalysts remains unchanged (5), the observed changes in selectivity could be explained on the basis of secondary reactions in the Fischer–Tropsch system. With increasing zirconium content the number of surface metal atoms at steady-state conditions increases, leading to a higher extent of secondary reactions, but the size of the cobalt clusters decreases, leading to a decrease in the extent of secondary reactions. With increasing zirconium content the extent of secondary hydrogenation of olefins (e.g., ethene) passes a minimum, and the $C_{5+}$-selectivity passes a maximum due to readsorption of small, reactive organic product compounds, which can be incorporated in larger product compounds. Double bond isomerization increases with increasing zirconium content. This might be attributed to the catalytic activity of zirconia.

## ACKNOWLEDGMENTS

The authors thank SASOL and THRIP for financial support for this research project. Furthermore, MC gratefully acknowledges a postdoctoral fellowship from UCT.

## REFERENCES

1. Fischer, F., Tropsch, H., and Dilthes, D., *Brennstoff-Chemie* **6**, 265 (1925).
2. Vannice, M. A., *J. Catal.* **50**, 228 (1977).
3. Schulz, H., van Steen, E., and Claeys, M., *Stud. Surf. Sci. Catal.* **81**, 204 (1994).
4. Igleasia, E., Soled, S. L., and Fiato, R. A., *J. Catal.* **137**, 212 (1992).
5. Iglesia, E., *Appl. Catal. A* **161**, 59 (1997).
6. Arnoldy, P., and Moulijn, J. A., *J. Catal.* **93**, 38 (1985).
7. Okamato, Y., Nagata, K., Adachi, T., Imanaka, T., Inamura, K., and Takyu, T., *J. Phys. Chem.* **95**, 310 (1991).
8. Rosynek, M. P., and Polansky, C. A., *Appl. Catal.* **73**, 97 (1991).
9. Puskas, I., Fleisch, T. H., Hall, J. B., Meyers, B. L., and Rochinski, R. T., *J. Catal.* **134**, 615 (1992).
10. Ming, H., and Baker, B. G., *Appl. Catal. A* **123**, 23 (1995).
11. Coulter, K. E., and Sault, A. G., *J. Catal.* **154**, 56 (1995).
12. Van Steen, E., Sewell, G. S., Makhote, R. A., Micklethwaite, C., Manstein, H., de Lange, M., and O'Connor, C. T., *J. Catal.* **162**, 220 (1996).
13. Khodakov, A. Y., Lynch, J., Bazin, D., Rebours, B., Zanier, N., Moisson, B., and Chaumette, P., *J. Catal.* **168**, 16 (1997).
14. Cheng, Z. X., Louis, C., and Che, M., *Z. Phys. D* **20**, 445 (1991).
15. Adesina, A. A., *Appl. Catal. A* **138**, 345 (1996).
16. Hoek, A., Minderhoudt, J. K, Post, M. F., and Lednor, P. W., EP 110449 A1 (1984).
17. Withers, H. P., Jr., Eliezer, K. F., and Mitchell, J. W., *Ind. Eng. Chem. Res.* **29**, 1807 (1990).
18. Ali, S., Chen, B., and Goodwin, J. G., *J. Catal.* **157**, 35 (1995).
19. Nie, Z., Ph.D. thesis, Univ. of Karlsruhe, 1997.
20. Reuel, R. C., and Bartholomew, C. H., *J. Catal.* **85**, 63 (1984).
21. Chin, R. L., and Hercules, D. M., *J. Phys. Chem.* **86**, 360 (1986).

22. Schulz, H., Böhringer, W., Rahman, N., Kohl, W., and Will, A., DGMK-Forschungsbericht 320, DGMK, Hamburg (1982).
23. "Gmehlin's Handbuch der anorganischen Chemie," Vol. 42, 8th ed. Verlag Chemie, Weinheim, 1958.
24. Schulz, H., Rao, B., and Elstner, M., *Erdöl Kohle* **22**, 651 (1970).
25. Van Steen, E., Ph.D. thesis, Univ. of Karlsruhe, 1993.
26. Schanke, D., Hilmen, A. M., Bergene, E., Kinnari, K., Rytter, E., Ådnanes, E., and Holmen, A., *Energy Fuels* **10**, 867 (1996).
27. Van Schalkwyk, E., Feller, A., Claeys, M., and van Steen, E., to be published.
28. Schulz, H., and Achtsnitt, H., *Rev. Port. Quim*. **19**, 317 (1977).
29. Kibby, C., Panell, R., and Kobylinsky, T., *Prepr. Am. Chem. Soc. Div. Pet. Chem*. **29**, 1113 (1984).
30. Wheeler, A., *in* "Advances in Catalysis III" (W. G. Frankenburg, E. K. Rideal, and V. I. Komarewsky, Eds.), p. 317, Academic Press, New York, 1951.